Seafloor topography and the thermal budget of Earth

Jun Korenaga[1]

Short title: SEAFLOOR TOPOGRAPHY AND EARTH'S THERMAL BUDGET

[1]Department of Geology and Geophysics, Yale University, New Haven, CT

Abstract. The subsidence of an aging seafloor starts to slow down at ∼70 Ma old with respect to the prediction of simple half-space cooling, and this phenomenon has long been known as seafloor flattening. The flattening signal remains even after removing the influence of the emplacement of hotspot islands and oceanic plateaus. The combination of small-scale convection and radiogenic heating has been suggested as a mechanism to explain seafloor flattening, and this study explores a possibility of using the magnitude of seafloor flattening to constrain the amount of radiogenic heating in the convecting mantle. By comparing properly scaled geodynamic predictions with the observed age-depth relation of the normal seafloor, the mantle heat production is estimated to be $\sim 12 \pm 3$ TW, which supports geochemistry-based estimates. A widely-held notion that small-scale convection enhances cooling thus being unable to explain seafloor flattening is suggested to be incorrect. The ability to predict the age-depth relation of seafloor based on the thermal budget of Earth has an important bearing on the future theoretical study of early Earth evolution.

INTRODUCTION

The evolution of oceanic lithosphere is one of the essential components in the theory of plate tectonics, yet it has long defied a clear physical explanation. What has been puzzling is the following: Seafloor topography, which reflects the thermal structure of oceanic lithosphere, starts to become shallower than the prediction of simple half-space cooling as seafloor becomes older than $\sim$70 Ma old [Parsons and Sclater, 1977; Stein and Stein, 1992] (Figure 1). Such deviation, often called seafloor flattening, can be modeled by the so-called plate model [Langseth et al., 1966; McKenzie, 1967], in which temperature at some shallow depth ($\sim$100 km) is fixed to a constant value. This boundary condition in the plate model, however, has no physical basis, which leads to the following frustrating situation. The half-space cooling model, which has a solid footing in the theory of thermal convection [Turcotte and Oxburgh, 1967], can explain seafloor topography only partially, whereas the plate model, which can explain the topography successfully, appears to be rather ad hoc from a physical perspective.

Efforts have been made to provide a physical mechanism for the upward deviation from half-space cooling, which requires the supply of heat from below in some way. The most commonly discussed mechanism is small-scale convection beneath oceanic lithosphere (also called as sublithospheric convection) [e.g., Parsons and McKenzie, 1978; Davaille and Jaupart, 1994; Dumoulin et al., 2001; Huang and Zhong, 2005; Afonso et al., 2008]. Some authors have discounted this possibility by arguing that small-scale convection would lead to more efficient cooling and be unable to supply additional heat [O'Connell and Hager, 1980; Davies, 1988b], but this seemingly reasonable argument does not hold with the typical time scale of oceanic lithosphere (see Discussion). Indeed, more recent studies suggest that the operation of small-scale convection in the presence of internal heat production may be sufficient to explain the flattening [e.g., Huang and Zhong, 2005]. Given our understanding of mantle rheology [Karato and Wu, 1993; Hirth and Kohlstedt, 2003], small-scale convection is dynamically feasible beneath oceanic lithosphere [Korenaga and Jordan, 2002a], and the convecting mantle contains radioactive isotopes [e.g., Jochum et al., 1983], the decay of which results in internal

heat production. A satisfactory model for the evolution of oceanic lithosphere could, therefore, be built with small-scale convection and internal heat production, and seafloor topography may be intimately connected to the thermal budget of Earth. For a variety of reasons that will be explained later, however, this connection is difficult to extract from previous studies, and it is the purpose of this paper to elucidate the relation between seafloor topography and the thermal budget of Earth, based on the proper scaling of fluid mechanics.

One may question the significance of the so-called flattening signal, because the majority of 'normal' seafloor unaffected by the emplacement of hotspot islands and oceanic plateaus is younger than 70 Ma old and can thus be explained by simple half-space cooling [Korenaga and Korenaga, 2008] (Figure 1). Also, even at older ages, there exists some seafloor that follows the half-space cooling trend. The discussion of the flattening signal is thus always in danger of the law of small numbers [e.g., Davies, 1988a; Sleep, 2011]. At the same time, it is important to realize that the concept of half-space cooling was originally developed on the basis of basally-heated convection (i.e., no internal heating) [Turcotte and Oxburgh, 1967], and in the presence of radioactive isotopes, mantle cooling does not have to follow half-space cooling in its purest form [e.g., Jarvis and Peltier, 1982]. Developing a physically sound model that can explain the faint flattening signal is therefore important, and this importance would be further amplified when considering seafloor topography in the Precambrian because internal heat production was certainly higher and seafloor might have survived longer than present [Korenaga, 2008a]. Seafloor topography controls the capacity of ocean basins, so having a physical model is essential for predicting the relative sea level — one of the key elements for the coevolution of the surface environment and the Earth's interior [e.g., Korenaga, 2013] — in the distant past. A phenomenological model that is fit to the present-day situation cannot be extrapolated for such a purpose.

The structure of this paper is as follows. After describing a strategy to simulate the transient cooling of the oceanic mantle, how to relate numerical results with actual Earth observations by dimensionalization is explained. As all of relevant model parameters suffer from some degree of uncertainty, an extensive grid search is conducted to identify a subset of model parameters that can explain seafloor flattening. A simple theoretical analysis is also

presented to help the interpretation of the search result. Previous studies on the evolution of oceanic lithosphere are then reviewed in light of new findings. Many authors have considered seafloor topography and oceanic heat flow jointly [e.g., Parsons and Sclater, 1977; Stein and Stein, 1992], but this paper places an emphasis on topography because heat flow data are not particularly diagnostic. The limitation of heat flow data is explained there in some detail. After this critique of previous studies, the relevance of the modeling results to surface wave tomography and early Earth issues is discussed, along with the significance of realistic mantle rheology. The paper ends with some prospects for future development.

THEORETICAL FORMULATION

Modelling Strategy

It may be ideal to simulate the dynamics of the oceanic mantle in a fully 3-D manner, but I choose to adopt a much simpler way to construct a ridge-perpendicular cross-section by horizontally averaging snapshots from a 2-D ridge-parallel model (Figure 2). By calculating instantaneous Stokes flow for the ridge-perpendicular thermal structure, seafloor topography can be calculated as a function of age [e.g., Davies, 1988c]. There are four reasons for this simplified approach. First, conducting fully 3-D simulation is deemed too excessive because creating a 2-D ridge-perpendicular cross-section is sufficient to calculate an age-depth relation. Second, 3-D models would also be too time-consuming when testing a range of model parameters in a systematic manner. In fact, even running 2-D convection models becomes very time-consuming for the grid search that is described later, and I have developed an efficient approximate method to directly compute the evolution of a horizontally-averaged thermal structure (see Appendix). Third, the interaction between plate-driven shear and small-scale convection is expected to give rise to the formation of longitudinal convection rolls [e.g., Richter, 1973; Richter and Parsons, 1975; Korenaga and Jordan, 2003a], so the dynamics of small-scale convection is well captured by 2-D ridge-parallel models [e.g., Buck and Parmentier, 1986; Korenaga and Jordan, 2004]. Finally, by constructing a ridge-perpendicular thermal structure as a composite of horizontally-averaged temperature

profiles, the dynamics of oceanic lithosphere can be isolated from other complications as such return flow associated with subduction. This two-step approach is better than directly running a 2-D ridge perpendicular model, in which plate-driven shear tends to delay the onset of sublithospheric convection [Huang et al., 2003].

The following non-dimensionalized equations are solved to track the evolution of a ridge-parallel cross section: (1) the conservation of mass,

$$\nabla \cdot \mathbf{u}^* = 0, \tag{1}$$

(2) the conservation of momentum,

$$-\nabla P^* + \nabla \cdot [\eta^* (\nabla \mathbf{u}^* + \nabla \mathbf{u}^{*T})] + RaT^* \mathbf{e}_z = 0, \tag{2}$$

and (3) the conservation of energy,

$$\frac{\partial T^*}{\partial t^*} + \mathbf{u}^* \cdot \nabla T^* = \nabla^2 T^* + H^*. \tag{3}$$

The unit vector pointing upward is denoted by $\mathbf{e}_z$. The spatial coordinates are normalized by the mantle thickness D, and time is normalized by the diffusion time scale, D^2/κ, where κ is thermal diffusivity. Velocity $\mathbf{u}^*$ is thus normalized by κ/D. Temperature is normalized by the temperature scale ΔT, and viscosity is by a reference viscosity η_0 at $T^* = 1$. Dynamic pressure P^* and heat generation H^* are normalized by $\eta_0 \kappa/D^2$ and $k\Delta T/(\rho_{m,0} D^2)$, respectively, where $\rho_{m,0}$ is reference mantle density and k is thermal conductivity. The Rayleigh number Ra is defined as

$$Ra = \frac{\alpha \rho_{m,0} g \Delta T D^3}{\kappa \eta_0}, \tag{4}$$

where α is thermal expansivity and g is gravitational acceleration. These governing equations are based on the Boussinesq approximation [e.g., Schubert et al., 2001], so the model temperature corresponds to potential temperature (hypothetical temperature of mantle adiabatically brought to the surface without melting).

The following linear-exponential viscosity is employed:

$$\eta^*(T^*) = \exp[\theta(1-T^*)]. \tag{5}$$

Here θ is the Frank-Kamenetskii parameter, which can be related to the activation energy of mantle rheology, E, as [e.g., Solomatov and Moresi, 2000]

$$\theta = \frac{E\Delta T}{R(T_s+\Delta T)^2}, \tag{6}$$

where R is the universal gas constant and T_s is the surface temperature. An 'effective' activation energy for the temperature-dependency of upper mantle viscosity is likely to be $\sim$300 kJ mol^{-1} regardless of creep mechanisms [Christensen, 1984; Korenaga, 2006; Korenaga and Karato, 2008], which is equivalent to θ of $\sim$18.5 with T_s of 273 K and ΔT of 1350 K.

The top and bottom boundaries are free slip. The top temperature is fixed to 0, and the bottom boundary is insulating. A reflecting boundary condition, i.e., free slip and insulating, is applied to the side boundaries. The aspect ratio of the model is four to reduce wall effects, and the model is discretized by 400×100 uniform quadrilateral elements. Internal temperature is set to 1 at $t^*=1$, with random perturbation with the amplitude of 10^{-5}. Because of the insulating bottom boundary, there are no upwelling plumes in the model, which allows us to focus on the intrinsic dynamics of oceanic lithosphere. The governing equations are solved by the finite element code of Korenaga and Jordan [2003b], with the Courant factor of 0.05 to accurately measure the onset time of small-scale convection. With $D = 2.9\times10^6$ m and $\kappa = 10^{-6}$ m^2 s^{-1}, the maximum seafloor age of 170 Ma corresponds to $t^* = 6.37\times10^{-4}$, and the model is run up to this time.

For each snapshot of a ridge-parallel model, a horizontally-averaged temperature profile, $\langle T^*\rangle$, is calculated, and non-dimensional surface heat flux is then calculated as

$$q^*(t^*) = \left.\frac{\partial\langle T^*\rangle}{\partial z^*}\right|_{z^*=0}. \tag{7}$$

By assembling a suite of $\langle T^* \rangle$, a ridge-perpendicular cross-section is constructed with an prescribed plate velocity so that the evolution of oceanic lithosphere up to a certain time can be contained in a model domain. Two aspect ratios (2 and 4) are tested, and in terms of predicted surface topography, difference is negligible, so the aspect ratio of 2 is adopted for the ridge-perpendicular model. Instantaneous Stokes flow for a given ridge-perpendicular model is calculated by solving the conservation of mass and momentum [equations (1) and (2)], with all boundaries being free slip [e.g., Davies, 1988c]. Non-dimensional surface topography is then obtained from non-dimensional normal stress acting on the surface as

$$h^* = -\frac{1}{Ra}\, \sigma^*_{zz}\big|_{z^*=0}. \tag{8}$$

The topography is first obtained as a function of distance from the ridge, and then converted to a function of seafloor age using the prescribed velocity.

In this study, the uniform distribution of internal heat production throughout the whole mantle is assumed for the sake of simplicity. There may be a deep reservoir enriched in heat-producing isotopes above the core-mantle boundary [e.g., Boyet and Carlson, 2005], but it is unlikely for such a deep heat source to affect the evolution of oceanic lithosphere. Also note that geochemical arguments for the presence of a deep enriched reservoir are logically flawed [Korenaga, 2009b]; a chemically distinct reservoir can exist in the lower mantle, but it is not necessarily enriched. Mantle melting beneath mid-ocean ridges differentiates the source mantle into enriched oceanic crust and depleted mantle lithosphere, but this depth-dependent heat production would not influence the dynamics of sublithospheric convection. Mantle melting also introduces dehydration stiffening [Hirth and Kohlstedt, 1996], which is not modeled by the assumed viscosity function [equation (5)], but fortunately, the effect of dehydration stiffening on the convective instability of oceanic lithosphere is negligible at the present-day condition [Korenaga, 2003]. Though the viscosity structure of the mantle is likely to be stratified [e.g., Hager et al., 1985; King, 1995], such realistic complication is not considered in this study. The study of Huang and Zhong [2005] suggests that stratified viscosity as well as phase changes do not have significant influence on surface topography.

The secular cooling of Earth could give rise to a virtual heat source at regional scales, because relatively uncooled regions may be considered to be warmed up when the average internal temperature is decreasing. Supercontinental insulation is a well-known example [Anderson, 1982; Korenaga, 2007b]. Such 'insulation' effect for the oceanic mantle is probably minor because a typical oceanic mantle is not isolated from convective mixing. When one simulates mantle convection in a closed model domain, however, it is easy to insulate the mantle beneath old oceanic lithosphere because large-scale circulation developed in a model brings subducted cold materials directly to a sub-ridge mantle. Huang and Zhong [2005] called this uncooled state beneath old lithosphere as 'trapped heat', but this phenomenon appears only when such a simple circulation from a subduction zone to a ridge is maintained for a sufficiently long time. On the real Earth, the geometry of plate boundaries is constantly evolving, and subducted materials do not necessarily return to their parental ridges. The significance of trapped heat in the oceanic mantle is thus unclear. Ridge-perpendicular models in this study are devoid of subduction to prevent the development of trapped heat.

Dimensionalization

Non-dimensional surface topography h^* may be dimensionalized as

$$h = a_h + b_h h^*, \tag{9}$$

where a_h is a bias and b_h is the topography scale defined as

$$b_h = \alpha \Delta T D \frac{\rho_{m,s}}{\rho_{m,s} - \rho_w}. \tag{10}$$

Here $\rho_{m,s}$ and ρ_w denote surface mantle density and water density, respectively. The bias is needed here to take into account the convention used for Earth's topography (i.e., measured with respect to the sea level). The topography scale suffers from nontrivial uncertainty. Laboratory measurements indicate that thermal expansivity for oceanic lithosphere is probably $\sim 3.5 \times 10^{-5}$ K^{-1} [e.g., Bouhifd et al., 1996; Jackson et al., 2003], but likely viscoelastic

effects may reduce it to $\sim 3.0 \times 10^{-5}$ K^{-1} [Korenaga, 2007a]. The potential temperature of the ambient mantle is estimated to be $\sim 1350 \pm 50$ °C based on petrology [Herzberg et al., 2007] and ~1400 °C based on mineral physics and seismology [Anderson, 2000]. With $D = 2.9 \times 10^6$ m, $\rho_{m,s} = 3300$ kg m^{-3}, and $\rho_w = 1000$ kg m^{-3}, the topography scale can thus be anywhere from $\sim 1.6 \times 10^5$ m to $\sim 2.0 \times 10^5$ m (Figure 3).

Given this uncertainty in the topography scale and the need to find the bias component, I choose to determine both parameters by the least squares regression of equation (9). The topography of the normal seafloor (based on the correlation criterion developed by Korenaga and Korenaga [2008]) is used for the left-hand side of equation (9), and the regression is weighted with areas corresponding to given age-depth pairs. The regression is limited for seafloor ages between 10 Ma and 70 Ma old; computed topography is unreliable for ages smaller than 10 Ma old because lithosphere near the ridge is too thin to be accurately represented by the adopted discretization, and actual topography deviates from the simple half-space cooling trend for ages greater than ~70 Ma. After determining a_h and b_h, computed topography and actual topography are compared for all ages greater than 10 Ma old to derive an average misfit. A given ridge-perpendicular thermal structure may be regarded as acceptable if it yields a small topography misfit and a physically plausible topography scale.

Similarly, non-dimensional surface heat flow can be dimensionalized as

$$q = b_q q^*, \tag{11}$$

where

$$b_q = k\frac{\Delta T}{D}. \tag{12}$$

As thermal conductivity k depends on temperature [Hofmeister, 1999], the conductivity in the above equation is best regarded as an effective value representing the entire lithosphere. The heat flow scale b_q is determined by fitting equation (11) with $q = 550/\sqrt{t}$ (where q is in mW m^{-2} and t in Ma old) [Korenaga and Korenaga, 2008] for ages smaller than 70 Ma. With this scale fixed, the non-dimensional internal heat production H^* may be converted to the total

heat production within the convecting mantle as:

$$H_m = \frac{b_q H^* M_m}{\rho_{m,0} D}, \tag{13}$$

where M_m is the mass of the mantle (4×10^{24} kg).

RESULTS

The convection model described previously is characterized by three nondimensional parameters, Ra, θ, and H^*. In this section, the model space is searched for the optimal combination(s) of these parameters so that topography and heat flow data are satisfied with reasonable material properties. An extensive grid search is first conducted in which the computation of a 2-D ridge-parallel model is done in an approximated manner. The evolution of a ridge-parallel model is computed next, only for optimal model parameters.

Grid Search

The ranges of the model parameters to be explored are as follows: $Ra = 10^{8.5}$ to 10^{10}, $\theta = 15$ to 25, and $H^* = 0$ to 30. The range of the Rayleigh number corresponds to the reference viscosity of $\sim 9 \times 10^{18}$ Pa s to $\sim 3 \times 10^{17}$ Pa s, and that of the Frank-Kamenetskii parameter to the activation energy of $\sim$240 kJ mol^{-1} to $\sim$400 kJ mol^{-1}. The upper limit on the non-dimensional heat production corresponds to the total heat production of $\sim$18 TW. These parameters are scanned with the following increments: $d \log_{10} Ra = 0.1$, $d\theta = 1$, and $dH^* = 1$, so the number of all parameter combinations is $\sim$5500. Because of this large number of combinations to be tested, ridge-perpendicular cross-sections are prepared with an approximate method (see Appendix). In addition to the topography misfit and the dimensionalization parameters such as a_h, b_h, and b_q, the onset time of sublithospheric convection is measured.

An example of model prediction is given in Figure 4. With $Ra = 10^{9.4}$ and $\theta = 18$, sublithospheric convection takes place at the age of $\sim$70 Ma old, and even without internal heat production ($H^* = 0$), seafloor topography starts to deviate from the half-space cooling

trend (Figure 4a). The degree of deviation increases for greater H^*, and the topography misfit decreases from 478 m at $H^* = 0$ to 430 m at $H^* = 25$. Even for ages smaller than 70 Ma old, the topography of normal seafloor comes with one standard deviation of $\sim$400 m [Korenaga and Korenaga, 2008], and for comparison, a topography misfit with the GDH1 plate model [Stein and Stein, 1992] is $\sim$430 m. Given this scattered nature of topography data, therefore, reducing the misfit down to $\sim$430 m is roughly equivalent to explaining the so-called flattening signal. In contrast, heat flow prediction hardly changes with H^* (Figure 4b). This is expected because the amount of internal heat production is not large enough to affect surface heat flux during the life time of oceanic lithosphere. The delamination of lithosphere by small-scale convection has a greater effect, and it can be seen that the operation of small-scale convection shifts heat low slightly upward by $\sim$3 mW m^{-2} with respect to purely half-space cooling (Figure 1c), resulting in a better fit to the high-quality heat flow data compiled by Nagihara et al. [1996].

Representative grid search results are shown in Figure 5. The most salient feature is that, as H^* increases, the topography misfit decreases and at the same time, the topography scale increases. This is because the cumulative effect of internal heat production acts to offset the effect of surface cooling. Another trend to be seen is the onset time of small-scale convection decreases for higher Ra and lower θ, as expected from the scaling law for the onset of convection with temperature-dependent viscosity [Korenaga and Jordan, 2003b; Huang et al., 2003]. The trade-off between the topography misfit and the topography scale can be better seen in Figure 6. To reduce the misfit down to $\sim$430 m while maintaining the scale within $1.8 \pm 0.2 \times 10^5$ m, the non-dimensional internal heat production has to be around 20 ± 5. This range of acceptable H^* is relatively insensitive to Ra and θ, but these two parameters have to be properly chosen so that the onset of convection takes places at $\sim$70 Ma old, e.g., $\theta = 15$ for $Ra = 10^{9.3}$, $\theta = 18$ for $Ra = 10^{9.4}$, and $\theta = 21$ for $Ra = 10^{9.5}$. The heat flow scale b_q is found to be $\sim$1.88 mW m^{-2} (corresponding to $k = \sim 4$ W m^{-1} K^{-1} with ΔT of 1350 K) for all of those optimal model parameters. As seen in Figures 5 (right column) and 6d, the onset time is only weakly sensitive to H^*; internal heat production does not have enough time to affect the thermal structure of a growing lithosphere in a significant way.

With the heat flow scale of $\sim$1.88 mW m^{-2} and the reference mantle density $\rho_{m,0}$ of 4300 kg m^{-3}, the optimal H^* of 20$\pm$5 corresponds to the total mantle heat production of 12$\pm$3 TW. This range of heat production is in agreement with 8.5 ± 5.5 TW, which is the estimate of heat production in the convecting mantle based on the chemical composition model of Earth [Korenaga, 2008b, Table 1]. The amount of internal heat production required to explain seafloor flattening is, therefore, consistent with the present-day thermal budget of Earth.

A Close Look

The 2-D ridge-parallel model is run for a few dozens of optimal combinations of model parameters to validate the approximate approach taken during the grid search. In general, the variation of surface topography with seafloor age is smoother for 2-D calculations (Figure 7), because the delamination of lithosphere does not take place instantaneously (see Appendix), but the overall amplitude of seafloor flattening is accurately modeled by the approximate approach. The two approaches yield nearly identical heat flow predictions, because surface heat flux is not very sensitive to the dynamics of the lower part of lithosphere.

Some snapshots of the temperature field are shown in Figure 8 for the case of $Ra = 10^{9.3}$, $\theta = 18$, and $H^* = 20$. With this value of θ, the temperature scale involved in sublithospheric convection is $\sim$50-100 K, and it gradually decreases with time because of internal heating. Also shown in Figure 8 is corresponding surface topography, which is informative of the scale of sublithospheric convection. Shortly after the onset of convection, the amplitude of topographic fluctuation is quite small, on the order of 10 m (Figure 8a), but it eventually grows to $\sim$100 m (Figure 8d) as the seafloor matures. Sublithospheric convection is initially small-scale, but grows to mantle-wide flow [e.g., Korenaga and Jordan, 2004], and this is indicated by the poorer correspondence between surface topography and lithospheric structure at later times. Part of scatters seen in the age-depth relation for the normal seafloor must originate in this type of topography variation induced by large-scale mantle flow [Kido and Seno, 1994].

Ridge-perpendicular cross-sections based on 2-D calculations are shown in Figure 9

for three optimal cases. For these cases, most of deviation from half-space cooling takes place below the contour of 1100 °C (note: this is potential temperature). With the strong temperature-dependency that characterizes mantle rheology, the onset of sublithospheric convection can perturb only the lowermost fraction of oceanic lithosphere, so its influence on surface heat flow is limited in magnitude as well as delayed in time [Korenaga, 2009a]. Surface topography is sensitive to the entire thermal structure of lithosphere, but the scatters in the age-depth relation of the normal seafloor do not allows us to distinguish between different combinations of model parameters solely based on surface topography. There is a strong trade-off between Ra and θ, and our understanding of upper-mantle rheology is not good enough to pinpoint either parameter [Korenaga and Karato, 2008]. Surface-wave tomography may have a better potential, and it will be discussed later.

Order-of-Magnitude Analysis

As suggested by Huang and Zhong [2005] and demonstrated with Earth-like model parameters in the previous section, the combination of small-scale convection and internal heat production is sufficient to explain the seafloor flattening. The combination of Ra and θ is such that the onset of small-scale convection starts at $\sim$70 Ma, and an acceptable relation between Ra and θ can easily be derived from the scaling law for the onset of convection. The remaining model parameter H^* controls the thermal equilibration of delaminated lithospheric materials. An order-of-magnitude estimate on the proper amount of internal heat production may be derived by considering isostasy and thermal budget.

The topography of the normal seafloor appears to deviate from the half-space cooling trend around 70 Ma old, and the deviation reaches $\sim$1 km at 170 Ma old (Figure 1b). A simple isostasy argument leads to the following relation between a topography excess, δh, and the thickness of delaminated lithosphere, δL:

$$\delta L = \frac{\rho_{m,s} - \rho_w}{\alpha \delta T \rho_{m,s}} \delta h, \tag{14}$$

where δT is the temperature difference between the delaminated lithosphere and the

sublithospheric mantle (i.e., asthenosphere). With δT of 200 K and δh of 1 km, δL is $\sim$120 km.

The delamination of lithosphere takes place over the period of 100 Ma, which is denoted by δt here, so heat flux needed to thermally equilibrate delaminated materials is

$$q_1 \sim \frac{C_p \rho_{m,s} \delta T \delta L}{\delta t}, \tag{15}$$

where C_p is the specific heat of the mantle (assumed here to be 1 kJ K^{-1} kg^{-1}). Small-scale convection can disperse the cold delaminated materials throughout the mantle, so heat flux due to internal heat production H should scale to the mantle depth D as

$$q_2 \sim \rho_{m,0} D H. \tag{16}$$

By equating the above two heat fluxes, H is estimated to be $\sim 2 \times 10^{-12}$ W kg^{-1}, which is equivalent to H^* of $\sim$13. This estimate serves as a lower bound because the mixing of delaminated materials by small-scale convection is unlikely to be as efficient as assumed. The optimal value of $H^* = 20$ may be derived by reducing the mantle depth D in equation (16) by $\sim$30%. This mixing effect, which allows access to whole-mantle heat production, is absent in the classical evolution model of oceanic lithosphere with internal heat production [e.g., Forsyth, 1977].

Heat fluxes discussed in the above, which are on the order of 20 mW m^{-2}, are both related to sublithospheric depths, and they do not have to be reflected in surface heat flux. The diffusion time scale for 100-km-thick lithosphere is $\sim$300 Ma, so oceanic lithosphere would subduct before thermal perturbations to the bottom of lithosphere are fully felt at the surface. For example, heat-flow difference between the half-space cooling and plate models is about 4 mW m^{-2} on average for seafloor older than 110 Ma old (Figure 1c), and by multiplying the area of the corresponding seafloor ($\sim 5 \times 10^7$ km^2), one obtains the heat production of $\sim$0.2 TW, which is substatially smaller than heat production in the convecting mantle. Though it may sound paradoxical, the thermal budget of Earth is more faithfully manifested in seafloor

topography than in surface heat flow.

DISCUSSION

Comments on Previous Studies

There have been a number of papers written on the origin of seafloor flattening in the past four decades. Many of them are concerned with distinguishing between the half-space cooling model and the plate model, or with elaborating on the specifics of the plate model, by comparing model predictions with topography and/or heat flow data [e.g., Davis and Lister, 1974; Parsons and Sclater, 1977; Stein and Stein, 1992; Carlson and Johnson, 1994; Hillier and Watts, 2005; Crosby et al., 2006; Zhong et al., 2007; Goutorbe and Hillier, 2013; Hasterok, 2013]. The plate model can easily explain the flattening behavior because the thickness of an aging lithosphere converges to a prescribed value imposed by the bottom boundary condition, typically set at the depth of $\sim$100 km. Because there is no such boundary in the Earth's mantle, however, fitting the plate model to seafloor data is not a meaningful exercise, unless the boundary condition can be justified as an approximation of some other physical mechanism. A similar comment applies to the constant bottom heat flux model [e.g., Crough, 1975; Doin and Fleitout, 1996], which is another kind of conduction model.

The long-standing popularity of conduction models in the literature has probably two reasons. First, it is much easier to compute the prediction of a conduction model than to simulate a fully dynamic calculation. Second, more dynamical approaches in the past have trod on a rather tortuous path, so they may appear confusing on first glance. For example, the role of small-scale convection in seafloor flattening was discounted by O'Connell and Hager [1980], who argued that the operation of convection means more efficient cooling so that seafloor would subside faster rather than slower. While it is true that a convecting system cools faster, on average, than a purely conducting system, cooling rates can be different at different depths (Figure 10). Because surface topography is more sensitive to the temperature of shallower depths, it is not evident that the onset of small-scale convection should immediately lead to a faster subsidence. In fact, results in this study show that the onset of convection

can slow down seafloor subsidence even without internal heat production (Figure 4a). It is important to study such a transient behavior with a model setting appropriate for Earth's mantle. Davies [1988b] supported the suggestion of O'Connell and Hager [1980], but his convection models used only weakly temperature-dependent viscosity, which prevents the direct application of his results to Earth's mantle. Strongly temperature-dependent viscosity has long been suggested to be important for the dynamics of lithosphere [e.g., Fleitout and Yuen, 1984; Davaille and Jaupart, 1994], but a correct scaling law for the onset of convection was not available until early 2000s [Korenaga and Jordan, 2003b; Huang et al., 2003].

The study of Huang and Zhong [2005] was a major step forward regarding the importance of small-scale convection and internal heat generation, but they placed an emphasis on building a steady-state convection model. In steady-state convection models, internal heat generation includes contributions from radioactive isotopes as well as secular cooling, and it is impossible to isolate the effect of radiogenic heating. Also, the temperature dependency of viscosity was still not high enough ($\theta \sim 6$ in their key results), so their conclusions can be appreciated only on a qualitative ground. Later attempts by Zlotnik et al. [2008] and Afonso et al. [2008] explored more realistic mantle rheology, but they did not quantitatively compare model predictions with actual data. Having an upward deviation from the half-space cooling trend does not constrain by itself the amount of internal heating (e.g., Figure 4a). It is the magnitude of the deviation that matters. The amount of radiogenic heating used in their models is equivalent to the total heat production of $\sim$20 TW, which is appropriate for the primitive mantle [e.g., McDonough and Sun, 1995; Lyubetskaya and Korenaga, 2007a], but not for the present-day convecting mantle [Lyubetskaya and Korenaga, 2007b].

When considering the role of small-scale convection in seafloor flattening, it is critical to focus on the observations of 'normal' seafloor. Seafloor flattening can be caused by both intrinsic and extrinsic causes, and small-scale convection belongs to the former. An obvious extrinsic cause is the emplacement of hotspot islands and oceanic plateaus [Heestand and Crough, 1981; Schroeder, 1984; Smith and Sandwell, 1997], and most of previous studies have been casual about how to exclude anomalous seafloor affected by such igneous activities. The correlation criterion developed by Korenaga and Korenaga [2008] (Figure 1a) is an effort

to identify the distribution of normal seafloor in an objective manner. When evaluating the success of a given convection model in this study, the age-depth data of the normal seafloor according to the correlation criterion are directly compared with model predictions (see Dimensionalization). The calculation of the topography misfit is weighted with areas for given age-depth pairs, to fully account for the statistical distribution of age-depth data.

A similar approach cannot be used for heat flow data, because of the paucity of reliable heat flow data. Heat flow at young seafloor is known to be considerably modified by hydrothermal circulation, but even at old seafloor, it is still difficult to obtain high-quality heat flow data. Heat flow from old seafloor is typically on the order of 50 mW m^{-2}, which translates to the temperature difference of about 0.1 K over a few-meter-long heat-flow probe. Securing an accuracy of a few percent thus requires multi-penetration measurements with in situ thermal conductivity or deep sea drilling backed up by surface surveys. Nagihara et al. [1996] reviewed then-available heat flow data and were able to identify only 14 reliable data over $>$100-Ma-old seafloor away from hotspots and oceanic plateaus. Four of them (sites F, H, I, and N in Table 1 of Nagihara et al. [1996]) are actually outside of the normal seafloor defined by Korenaga and Korenaga [2008], and the remaining 10 data do not exhibit a notable deviation from the half-space cooling trend (Figure 1c). The most recent compilation effort of Hasterok [2013] is not very useful because many data in the compilation reside in the anomalous seafloor identified by Korenaga and Korenaga [2008]; as one can clearly see in Figure 7 of Korenaga and Korenaga [2008], the area of normal seafloor older than 100 Ma old is insignificant. The same criticism applies to earlier compilation efforts [e.g., Stein and Stein, 1992]. The recent discovery of petit-spot volcanoes around the world [e.g., Hirano et al., 2006, 2013] implies that the definition of anomalous seafloor may be more extensive for heat flow because disturbing a local thermal gradient is easier than disturbing isostasy [Yamamoto et al., 2014]. Regarding the gross evolution of oceanic lithosphere, therefore, the utility of heat flow data is much more limited than that of topography data.

Surface Wave Tomography

Surface wave tomography is a promising tool to probe the thermal evolution of oceanic lithosphere more directly than surface topography and heat flow [e.g., Ritzwoller et al., 2004]. Any tomographic image, however, is a model based on observations and not an observation itself, so a greater care is needed when comparing with predictions from geodynamic modeling.

As indicated by Figure 9, explaining the seafloor flattening does not require to limit the thickness of lithosphere to $\sim$100 km. The 1100 $^{\circ}$C contour, which is often used as the base of lithosphere, follows closely the prediction of half-space cooling, being consistent with the findings of recent surface wave studies [e.g., Maggi et al., 2006; Debayle and Ricard, 2012]. These recent studies often present a tomographic cross-section stacked with respect to seafloor age, which exhibits intriguing small-scale deviations from the half-space cooling prediction. Such deviations, if real, can help distinguishing between different model parameters, so it is important to quantify the uncertainty of such a stacked image. Tomographic inversion requires regularization such as damping and smoothing, which introduces correlated uncertainty among velocity parameters. Such correlated uncertainty, i.e., model covariance, is rarely reported in the study of surface wave tomography, because properly estimating it is time-consuming [e.g., Shapiro and Ritzwoller, 2002] and because it is not practical to publish the covariance, which is an extremely large matrix. It is possible, however, to reduce the model covariance to a much more compact set of eigenmodes by the principal component analysis [Korenaga and Sager, 2012]. Such information would be essential if one wish to derive a different age stack by focusing on a particular region such as the ‘normal’ seafloor of Korenaga and Korenaga [2008]. Localizing an age stack to the normal seafloor is essential when considering intrinsic lithospheric dynamics, and quantifying its uncertainty would allow us to extract the most reliable information. Continuous methodological innovations [e.g., Schaeffer and Lebedev, 2013], coupled with rigorous uncertainty analysis, may eventually make surface wave tomography as decisive constraints on the evolution of oceanic lithosphere.

Realistic Mantle Rheology

The linear-exponential viscosity function used in this study [equation (5)] is Newtonian, i.e., viscosity is independent of stress. Realistic mantle rheology is, however, a combination of both Newtonian and non-Newtonian mechanisms, the former by diffusion creep and the latter by dislocation creep [Karato and Wu, 1993; Hirth and Kohlstedt, 2003]. The study of small-scale convection has commonly employed the linear-exponential viscosity, partly because it is sensible to solve simple problems first and partly because the simple viscosity function is believed to be sufficient to capture the first-order characteristics of mantle rheology. The use of linear-exponential viscosity introduces only one additional non-dimensional parameter (i.e., θ), which has considerably facilitated theoretical analysis. Owing to previous studies, the effect of linear-exponential viscosity on thermal convection is now well understood, and it may be time to consider the effect of realistic mantle rheology. The two deformation mechanisms (diffusion and dislocation) operate differently under dry and wet conditions, and sublithospheric dynamics is where all of these complications meet.

The consideration of both Newtonian and non-Newtonian mechanisms could potentially explain one puzzling feature of the age-depth relation (Figure 1b). As noted in Introduction, a small fraction of seafloor follows the half-space cooling trend, up to $\sim$100 Ma old, so there seem two branches of evolution after $\sim$70 Ma old, i.e., a flattening branch and a subsiding branch. Newtonian viscosity cannot explain this branching, because small-scale convection can be triggered by infinitesimal perturbations and all seafloor should experience flattening. In contrast, with non-Newtonian viscosity, the onset of convection depends on the amplitude of perturbations [Solomatov and Barr, 2007]. With a sufficiently quiet environment, therefore, oceanic lithosphere could continue to grow without experiencing convective instability. The significance of non-Newtonian rheology on small-scale convection may be most evident where strong perturbations are expected such as fracture zones [e.g., Cadio and Korenaga, 2014], but this study suggests that the age-depth relation of normal seafloor is also useful to constrain the role of non-Newtonian rheology. Lithospheric delamination becomes more efficient with non-Newtonian rheology [Sleep, 2002], which may lead to a better fit to the flattening branch.

In addition to this non-Newtonian issue, the depth dependence of viscosity owing to non-zero activation volume may also be important. The study of Huang and Zhong [2005] indicates that dynamic topography due to small-scale convection is only weakly sensitive to the lower mantle viscosity, and this is probability because small-scale convection is characterized with short wavelengths [cf. Wen and Anderson, 1997]. The effect of gradual increase in viscosity within the upper mantle, however, remains to be investigated. Unfortunately, activation volumes for upper-mantle rheology are among the most poorly constrained flow-law parameters [Korenaga and Karato, 2008], because of the difficulty of conducting deformation experiments at high pressures. Considering sublithospheric dynamics with realistic mantle rheology thus requires us to carefully evaluate modeling results by taking into account the uncertainty of rheological parameters [e.g., Chu and Korenaga, 2012].

Relevance to Early Earth Issues

To explain the observed age-depth relation of the present-day seafloor, the total heat production in the convecting mantle is estimated to be $\sim 12 \pm 3$ TW (see Grid Search). Heat losses from the oceanic and the continental mantle are estimated as $\sim$32 TW and $\sim$6.5 TW, respectively [Jaupart et al., 2007; Korenaga, 2008b], so the convective Urey ratio, which is the ratio of mantle heat production to mantle heat loss, is ~ 0.3. A similar estimate can be derived from geochemical consideration [McDonough and Sun, 1995; Lyubetskaya and Korenaga, 2007b]. To reconstruct a geologically acceptable thermal history of Earth with this low value of the Urey ratio, plate tectonics in the past should have been more sluggish than present, at least back to the Archean [Korenaga, 2003, 2006]. This theoretical prediction has since been corroborated by the life span of passive margins [Bradley, 2008], the cooling history of the upper mantle [Herzberg et al., 2010], the degassing history of xenon [Padhi et al., 2012], and the secular evolution of continental plate velocity [Condie et al., 2014]. More sluggish plate tectonics in the past was a radical notion when it was first suggested in 2003, but the above supporting data from disparate disciplines suggest that it is a reasonable approximation to the actual Earth history.

Slower plate motion in the past means that seafloor survives longer, and Korenaga

[2008a] estimated that the maximum seafloor age in the Archean might exceed 300 Ma old. It is possible to reduce the maximum age by assuming smaller plates, but such possibility can be discounted on the basis of the subductability of oceanic lithosphere [Korenaga, 2006]. Archean oceanic lithosphere is thus likely to have entertained a longer life span [e.g., Bradley, 2008], and seafloor could have been deeper than present on average. The amount of radiogenic heating in the mantle doubles in the Archean, so seafloor flattening could have been more enhanced in the past. At the same time, the effect of dehydration stiffening would be more pronounced when the mantle was hotter in the past, so the convective thinning of lithosphere tends to be suppressed [Korenaga, 2003]. It would be interesting to quantify the degree of seafloor flattening in the Archean by combining these competing factors: a longer time span, greater heat production, and a thicker dehydrated lithosphere.

Such consideration is of fundamental importance when modeling the long-term evolution of global sea level, because the age-depth relation of seafloor controls the capacity of ocean basins [e.g., Parsons, 1982; Korenaga, 2007b]. Previous studies on the plate model have suggested a range of equilibrium plate thickness, e.g., 125 km [Parsons and Sclater, 1977], 95 km [Stein and Stein, 1992], and 90 km [Hasterok, 2013], but what controls this thickness is always left unanswered. What fits the present-day seafloor does not necessarily work for seafloor at different times. This study is the first theoretical attempt to explain seafloor flattening with the thermal budget of Earth and realistic temperature-dependent viscosity, and we can finally extrapolate to deeper times with a theoretical justification.

In addition to the shape of ocean basins, the global sea level is affected by the total volume of surface water, the relative buoyancy of continental and oceanic lithosphere, and the surface partitioning of continental and oceanic crust [Korenaga, 2013]. So estimating the age-depth relation in the past is only a step forward, but it is an important step toward several outstanding problems in the early Earth, as the secular evolution of global sea level is intimately related to the activation of the global carbon cycle [e.g., Kasting and Catling, 2003] and the uprise of oxygen [e.g., Kump and Barley, 2007].

CONCLUDING REMARKS

By constructing a simple geodynamic model with Earth-like parameters and comparing model predictions with the age-depth relation of the normal seafloor, the so-called seafloor flattening is shown to have a constraint on the amount of radiogenic heating in the convective mantle. The estimated range of heat production, $\sim 12 \pm 3$ TW is consistent with independent geochemical estimates, providing yet another support to the present-day Urey ratio of $\sim$0.3.

This physical underpinning for the long-standing puzzle of present-day seafloor has an important bearing on the future theoretical study of early Earth evolution. At the same time, it is also necessary to examine the validity of various simplifications made in this study, such as the Boussinesq approximation and the use of effective material properties. Whole-mantle convection is assumed a priori in this study, but alternative ideas do exist [e.g., Tackley, 2000; Anderson, 2011]. Testing the significance of detailed mineral physics information is certainly warranted [e.g., Grose, 2012; Grose and Afonso, 2013], but more important, the dynamics of small-scale convection needs to be reassessed with realistic composite rheology. Because many rheological parameters are still poorly constrained [Korenaga and Karato, 2008], incorporating such uncertainty into future modeling efforts is as important as quantifying the uncertainty of seismic tomography models. Combining geodynamics and seismology to derive reliable constraints on the dynamic state of the mantle requires careful statistical consideration on both sides. Though indirect, such multidisciplinary efforts on the present-day lithospheric dynamics have a definite connection to the Earth history at large.

APPENDIX: APPROXIMATE MODELING OF HORIZONTALLY-AVERAGED THERMAL STRUCTURE

A horizontally-averaged temperature profile, $\langle T^* \rangle$, may be calculated by solving the following 1-D conduction equation:

$$\frac{\partial \langle T^* \rangle}{\partial t^*} = \frac{\partial^2 \langle T^* \rangle}{\partial z^{*2}} + H^*, \tag{A1}$$

which involves no approximation before the onset of convection. The convective stability of a growing thermal boundary layer is monitored by calculating the local Rayleigh number with the formalism of Korenaga and Jordan [2002b] at every time step, and when the local Rayleigh number exceeds a critical value, Ra_c, convection is assumed to instantly homogenize the thermal structure beneath the origin of available buoyancy, z_o^*. As convective mixing is expected to be more efficient when the effective Rayleigh number for the mixing region is higher, the temperature below z_o^* is updated as

$$\langle T^* \rangle (t^* + \Delta t^*, z^*) = (1-\beta)\langle T^* \rangle (t^*, z^*) + \beta T_m^*(t^*), \tag{A2}$$

where

$$T_m^*(t^*) = \frac{1}{1-z_o^*} \int_{z_o^*}^{1} \langle T^* \rangle (t^*, z^*) dz^*, \tag{A3}$$

and the under-relaxation parameter β is calculated as

$$\beta = \max(1, \min(0, 0.5 + c \log(Ra_e / Ra_{e,0}))), \tag{A4}$$

with the effective Rayleigh number defined as

$$Ra_e = Ra\, \delta T (1-z_o^*)^3 \exp[-\theta(1-T_m^*)]. \tag{A5}$$

Here δT is a total temperature contrast below z_o^* at t^*.

When the amplitude of initial temperature perturbations is 10^{-5}, the critical Rayleigh number Ra_c may be set as 2000 [Korenaga and Jordan, 2003b]. The parameters c and $Ra_{e,0}$ in equation (A4) need to be calibrated by comparing approximate solutions with corresponding 2-D numerical solutions. For this calibration purpose, a few dozens of 2-D solutions up to t^*=3 t_c^*, where t_c^* is the onset time of convection, were prepared with $Ra = 10^7$ to 10^9, $\theta = 10$ to 25, and $H^* = 3$ to 25. A grid search for the optimal parameter values yielded $c = 0.3$ and $Ra_{e,0} = 10^{6.5}$. This approximate method provides reasonably accurate predictions for surface topography and heat flow (with the root-mean-square error of $\sim$5%), when $Ra \geq 3 \times 10^7$ and

$\theta \geq 15$; this is because the assumption of instantaneous mixing becomes more justified when *Ra* is higher and the temperature contrast involved is lower.

Acknowledgments. Don Anderson suggested me to write on the thermal history of Earth or seafloor topography, and it was fortunate that I was ready with an idea to constrain the thermal budget of Earth from seafloor topography. Don was one of my few ‘spiritual’ mentors, whose work had tremendous impacts when I was striving to become an independent thinker. I am therefore very grateful for the editors for their invitation to this honor volume. Reviews from Carol Stein, Norm Sleep, and Scott King were helpful to improve the clarify of the manuscript.

References

Afonso, J.C., Zlotnik, S., and Fernandez, M., 2008, Effects of compositional and rheological stratifications on small-scale convection under the oceans: Implications for the thickness of oceanic lithosphere and seafloor flattening: Geophys. Res. Lett., v. 35, p. L20,308, doi:10.1029/2008GL035,419.

Anderson, D.L., 1982, Hotspots, polar wander, Mesozoic convection, and the geoid: Nature, v. 297, p. 391–393.

Anderson, D.L., 2000, The thermal state of the upper mantle; no role for mantle plumes: Geophys. Res. Lett., v. 27, p. 3623–3626.

Anderson, D.L., 2011, Hawaii, boundary layers and ambient mantle — geophysical constraints: J. Petrol., v. 52, p. 1547–1577.

Bouhifd, M.A., Andrault, D., Figuet, G., and Richet, P., 1996, Thermal expansion of forsterite up to the melting point: Geophys. Res. Lett., v. 23, p. 1143–1146.

Boyet, M., and Carlson, R.W., 2005, ^{142}Nd evidence for early (>4.53 Ga) global differentiation of the silicate Earth: Science, v. 309, p. 576–581.

Bradley, D.C., 2008, Passive margins through earth history: Earth-Sci. Rev., v. 91, p. 1–26.

Buck, W.R., and Parmentier, E.M., 1986, Convection beneath young oceanic lithosphere: Implications for thermal structure and gravity: J. Geophys. Res., v. 91, p. 1961–1974.

Cadio, C., and Korenaga, J., 2014, Resolving the fine-scale density structure of shallow oceanic mantle by Bayesian inversion of locaized geoid anomlaies: J. Geophys. Res. Solid Earth, v. 119, p. 3627–3645, doi:10.1002/2013JB010,840.

Carlson, R.L., and Johnson, H.P., 1994, On modeling the thermal evolution of the oceanic upper mantle: An assessment of the cooling model: J. Geophys. Res., v. 99, p. 3201–3214.

Christensen, U., 1984, Convection with pressure- and temperature-dependent non-Newtonian rheology: Geophys. J. R. Astron. Soc., v. 77, p. 343–384.

Chu, X., and Korenaga, J., 2012, Olivine rheology, shear stress, and grain growth in the lithospheric mantle: Geological constraints from the Kaapvaal craton: Earth Planet. Sci. Lett., v. 333-334, p. 52–62.

Condie, K., Pisarevsky, S., Korenaga, J., and Gardoll, S., 2014, Is the rate of supercontinent assembly changing with time?: Precambrian Res., v. in press.

Crosby, A.G., McKenzie, D., and Sclater, J.G., 2006, The relationship between depth, age and gravity in the oceans: Geophys. J. Int., v. 166, p. 443–573.

Crough, S.T., 1975, Thermal model of oceanic lithosphere: Nature, v. 256, p. 388–390.

Davaille, A., and Jaupart, C., 1994, Onset of thermal convection in fluids with temperature-dependent viscosity: Application to the oceanic mantle: J. Geophys. Res., v. 99, p. 19,853–19,866.

Davies, G.F., 1988a, Ocean bathymetry and mantle convection: 1. large-scale llow and hotspots: J. Geophys. Res., v. 93, p. 10,467–10,480.

Davies, G.F., 1988b, Ocean bathymetry and mantle convection: 2. small-scale flow: J. Geophys. Res., v. 93, p. 10,481–10,488.

Davies, G.F., 1988c, Role of the lithosphere in mantle convection: J. Geophys. Res., v. 93, p. 10,451–10,466.

Davis, E.E., and Lister, C.R.B., 1974, Fundamentals of ridge crest topography: Earth Planet. Sci. Lett., v. 21, p. 405–413.

Debayle, E., and Ricard, Y., 2012, A global shear wave velocity model of the upper mantle from fundamental and higher Rayleigh mode measurements: J. Geophys. Res., v. 117, p. B10,308, doi:10.1029/2012JB009,288.

Doin, M.P., and Fleitout, L., 1996, Thermal evolution of the oceanic lithosphere: an alternative view: Earth Planet. Sci. Lett., v. 142, p. 121–136.

Dumoulin, C., Doin, M.P., and Fleitout, L., 2001, Numerical simulations of the cooling of an oceanic lithosphere above a convective mantle: Phys. Earth Planet. Inter., v. 125, p. 45–64.

Fleitout, L., and Yuen, D.A., 1984, Secondary convection and the growth of the oceanic lithosphere: Phys. Earth Planet. Inter., v. 36, p. 181–212.

Forsyth, D.W., 1977, The evolution of the upper mantle beneath mid-ocean ridges: Tectonophysics, v. 38, p. 89–118.

Goutorbe, B., and Hillier, J.K., 2013, An integration to optimally constrain the thermal structure of oceanic lithosphere: J. Geophys. Res., v. 118, p. 432–446, doi:10.1029/2012JB009,527.

Grose, C.J., 2012, Properties of oceanic lithosphere: Revised plate cooling model predictions: Earth Planet. Sci. Lett., v. 333-334, p. 250–264.

Grose, C.J., and Afonso, J.C., 2013, Comprehensive plate models for the thermal evolution of oceanic lithosphere: Geochem. Geophys. Geosys., v. 14, p. 3751–3778, doi:10.1002/ggge.20,232.

Hager, B.H., Clayton, R.W., Richards, M.A., Comer, R.P., and Dziewonski, A.M., 1985, Lower mantle heterogeneity, dynamic topography and the geoid: Nature, v. 313, p. 541–545.

Hasterok, D., 2013, A heat flow based cooling model for tectonic plates: Earth Planet. Sci. Lett., v. 361, p. 34–43.

Heestand, R.L., and Crough, S.T., 1981, The effect of hot spots on the oceanic age-depth relation: J. Geophys. Res., v. 86, p. 6107–6114.

Herzberg, C., Asimow, P.D., Arndt, N., Niu, Y., Lesher, C.M., Fitton, J.G., Cheadle, M.J., and Saunders, A.D., 2007, Temperatures in ambient mantle and plumes: Constraints from basalts, picrites, and komatiites: Geochem. Geophys. Geosys., v. 8, no. 2, p. Q02,206, doi:10.1029/2006GC001,390.

Herzberg, C., Condie, K., and Korenaga, J., 2010, Thermal evolution of the Earth and its petrological expression: Earth Planet. Sci. Lett., v. 292, p. 79–88.

Hillier, J.K., and Watts, A.B., 2005, Relationship between depth and age in the North Pacific ocean: J. Geophys. Res., v. 110, p. B02,405, doi:10.1029/2004JB003,406.

Hirano, N., Machida, S., Abe, N., Morishita, T., Tamura, A., and Arai, S., 2013, Petit-spot lava fields off the central Chile trench induced by plate flexure: Geochem. J., v. 47, p. 249–257.

Hirano, N., Takahashi, E., Yamamoto, J., Machida, S., Abe, N., Ingle, S., Kaneoka, I., Hirata, T., Kimura, J., Ishii, T., and Ogawa, Y., 2006, Volcanism in response to plate flexure: Science, v. 313, p. 1426–1428.

Hirth, G., and Kohlstedt, D., 2003, Rheology of the upper mantle and the mantle wedge: A view from the experimentalists, *in* Eiler, J., ed., Inside the subduction factory: Washington, DC, American Geophysical Union, p. 83–105.

Hirth, G., and Kohlstedt, D.L., 1996, Water in the oceanic mantle: Implications for rheology, melt extraction, and the evolution of the lithosphere: Earth Planet. Sci. Lett., v. 144, p. 93–108.

Hofmeister, A.M., 1999, Mantle values of thermal conductivity and the geotherm from phonon lifetimes: Science, v. 283, p. 1699–1706.

Huang, J., and Zhong, S., 2005, Sublithospheric small-scale convection and its implications for residual topography at old ocean basins and the plate model: J. Geophys. Res., v. 110, p. B05,404, 10.1029/2004JB003,153.

Huang, J., Zhong, S., and Hunen, J.v., 2003, Controls on sublithospheric small-scale convection: J. Geophys. Res., v. 108, no. B8, p. 2405, doi:10.1029/2003JB002,456.

International Heat Flow Commission of IASPEI, 2011, Global heat flow database: URL `http://www.heatflow.und.edu/index2.html`.

Jackson, J.M., Palko, J.W., Andrault, D., Sinogeikin, S.V., Lakshtanov, D.L., Wang, J., Bass, J.D., and Zha, C.S., 2003, Thermal expansion of natural orthoenstatite to 1473 K: Eur. J. Mineral., v. 15, p. 469–473.

Jarvis, G.T., and Peltier, W.R., 1982, Mantle convection as a boundary layer phenomenon: Geophys. J. R. Astron. Soc., v. 68, p. 389–427.

Jaupart, C., Labrosse, S., and Mareschal, J.C., 2007, Temperatures, heat and energy in the mantle of the Earth, *in* Schubert, G., ed., Treatise on geophysics, v. 7: Amsterdam, Elsevier, p. 253–303.

Jochum, K.P., Hofmann, A.W., Ito, E., Seufert, H.M., and White, W.M., 1983, K, U and Th in mid-ocean ridge basalt glasses and heat production, K/U and K/Rb in the mantle: Nature, v. 306, p. 431–436.

Karato, S., and Wu, P., 1993, Rheology of the upper mantle: A synthesis: Science, v. 260, p. 771–778.

Kasting, J.F., and Catling, D., 2003, Evolution of a habitable planet: Annu. Rev. Astron. Astrophys., v. 41, p. 429–463.

Kido, M., and Seno, T., 1994, Dynamic topography compared with residual depth anomalies in oceans and implications for age-depth curves: Geophys. Res. Lett., v. 21, no. 8, p. 717–720.

King, S.D., 1995, Models of mantle viscosity, *in* Global earth physics: A handbook of physical constants: American Geophysical Union, p. 227–236.

Korenaga, J., 2003, Energetics of mantle convection and the fate of fossil heat: Geophys. Res. Lett., v. 30, p. 1437, doi:10.1029/2003GL016,982.

Korenaga, J., 2006, Archean geodynamics and the thermal evolution of Earth, *in* Benn, K., Mareschal, J.C., and Condie, K., eds., Archean geodynamics and environments: Washington, D.C., American Geophysical Union, p. 7–32.

Korenaga, J., 2007a, Effective thermal expansivity of Maxwellian oceanic lithosphere: Earth Planet. Sci. Lett., v. 257, p. 343–349.

Korenaga, J., 2007b, Eustasy, supercontinental insulation, and the temporal variability of terrestrial heat flux: Earth Planet. Sci. Lett., v. 257, p. 350–358.

Korenaga, J., 2008a, Plate tectonics, flood basalts, and the evolution of Earth's oceans: Terra Nova, v. 20, p. 419–439.

Korenaga, J., 2008b, Urey ratio and the structure and evolution of Earth's mantle: Rev. Geophys., v. 46, p. RG2007, doi:10.1029/2007RG000,241.

Korenaga, J., 2009a, How does small-scale convection manifest in surface heat flux?: Earth Planet. Sci. Lett., v. 287, p. 329–322.

Korenaga, J., 2009b, A method to estimate the composition of the bulk silicate Earth in the presence of a hidden geochemical reservoir: Geochim. Cosmochim. Acta, v. 73, p. 6952–6964.

Korenaga, J., 2013, Initiation and evolution of plate tectonics on Earth: Theories and observations: Annu. Rev. Earth Planet. Sci., v. 41, p. 117–151.

Korenaga, J., and Jordan, T.H., 2002a, On 'steady-state' heat flow and the rheology of oceanic mantle: Geophys. Res. Lett., v. 29, no. 22, p. 2056, doi:10.1029/2002GL016,085.

Korenaga, J., and Jordan, T.H., 2002b, Onset of convection with temperature- and depth-dependent viscosity: Geophys. Res. Lett., v. 29, no. 19, p. 1923, doi:10.1029/2002GL015,672.

Korenaga, J., and Jordan, T.H., 2003a, Linear stability analysis of Richter rolls: Geophys. Res. Lett., v. 30, no. 22, p. 2157, doi:10.1029/2003GL018,337.

Korenaga, J., and Jordan, T.H., 2003b, Physics of multiscale convection in Earth's mantle: Onset of sub-lithospheric convection: J. Geophys. Res., v. 108, no. B7, p. 2333, doi:10.1029/2002JB001,760.

Korenaga, J., and Jordan, T.H., 2004, Physics of multiscale convection in Earth's mantle: Evolution of sublithospheric convection: J. Geophys. Res., v. 109, p. B01,405, doi:10.1029/2003JB002,464.

Korenaga, J., and Karato, S., 2008, A new analysis of experimental data on olivine rheology: J. Geophys. Res., v. 113, p. B02,403, doi:10.1029/2007JB005,100.

Korenaga, J., and Sager, W.W., 2012, Seismic tomography of Shatsky Rise by adaptive importance sampling: J. Geophys. Res., v. 117, p. B08,102, doi:10.1029/2012JB009,248.

Korenaga, T., and Korenaga, J., 2008, Subsidence of normal oceanic lithosphere, apparent thermal expansivity, and seafloor flattening: Earth Planet. Sci. Lett., v. 268, p. 41–51.

Kump, L.R., and Barley, M.E., 2007, Increased subaerial volcanism and the rise of atmospheric oxygen 2.5 billion years ago: Nature, v. 448, p. 1033–1036.

Langseth, M.G., Le Pichon, X., and Ewing, M., 1966, Crustal structure of the mid-ocean ridges, 5, heat flow through the Atlantic ocean floor and convection currents: J. Geophys. Res., v. 71, p. 5321–5355.

Lyubetskaya, T., and Korenaga, J., 2007a, Chemical composition of Earth's primitive mantle and its variance, 1, methods and results: J. Geophys. Res., v. 112, p. B03,211, doi:10.1029/2005JB004,223.

Lyubetskaya, T., and Korenaga, J., 2007b, Chemical composition of Earth's primitive mantle and its variance, 2, implications for global geodynamics: J. Geophys. Res., v. 112, p. B03,212, doi:10.1029/2005JB004,224.

Maggi, A., Debayle, E., Priestley, K., and Barruol, G., 2006, Multimode surface waveform tomography of the Pacific Ocean: a closer look at the lithospheric cooling signature: Geophys. J. Int., v. 166, p. 1384–1397.

McDonough, W.F., and Sun, S.s., 1995, The composition of the Earth: Chem. Geol., v. 120, p. 223–253.

McKenzie, D.P., 1967, Some remarks on heat flow and gravity anomalies: J. Geophys. Res., v. 72, p. 6261–6273.

Nagihara, S., Lister, C.R.B., and Sclater, J.G., 1996, Reheating of old oceanic lithosphere: Deductions from observations: Earth Planet. Sci. Lett., v. 139, p. 91–104.

O'Connell, R.J., and Hager, B.H., 1980, On the thermal state of the earth, *in* Dziewonski, A., and Boschi, E., eds., Physics of the earth's interior: North-Holland, p. 270–317.

Padhi, C.M., Korenaga, J., and Ozima, M., 2012, Thermal evolution of Earth with xenon degassing: A self-consistent approach: Earth Planet. Sci. Lett., v. 341-344, p. 1–9.

Parsons, B., 1982, Causes and consequences of the relation between area and age of the ocean floor: J. Geophys. Res., v. 87, p. 289–302.

Parsons, B., and McKenzie, D., 1978, Mantle convection and the thermal structure of the plates: J. Geophys. Res., v. 83, p. 4485–4496.

Parsons, B., and Sclater, J.G., 1977, An analysis of the variation of ocean floor bathymetry and heat flow with age: J. Geophys. Res., v. 82, no. 5, p. 803–827.

Richter, F.M., 1973, Convection and the large-scale circulation of the mantle: J. Geophys. Res., v. 78, p. 8735–8745.

Richter, F.M., and Parsons, B., 1975, On the interaction of two scales of convection in the mantle: J. Geophys. Res., v. 80, p. 2529–2541.

Ritzwoller, M.H., Shapiro, N.M., and Zhong, S., 2004, Cooling history of the Pacific lithosphere: Earth Planet. Sci. Lett., v. 226, p. 69–84.

Schaeffer, A.J., and Lebedev, S., 2013, Global shear speed structure of the upper mantle and transition zone: Geophys. J. Int., v. 194, p. 417–449.

Schroeder, W., 1984, The empirical age-depth relation and depth anomalies in the Pacific ocean basin: J. Geophys. Res., v. 89, p. 9873–9883.

Schubert, G., Turcotte, D.L., and Olson, P., 2001, Mantle convection in the earth and planets: New York, Cambridge.

Shapiro, N.M., and Ritzwoller, M.H., 2002, Monte-Carlo inversion for a global shear velocity model of the crust and upper mantle: Geophys. J. Int., v. 151, p. 88–105.

Sleep, N.H., 2002, Local lithospheric relief associated with fracture zones and ponded plume material: Geochem. Geophys. Geosys., v. 3, p. 8506, doi:10.1029/2002GC000,376.

Sleep, N.H., 2011, Small-scale convection beneath oceans and continents: Chiense Sci. Bull., v. 56, p. 1292–1317.

Smith, W.H.F., and Sandwell, D.T., 1997, Global sea floor topography from satellite altimetry and ship depth soundings: Science, v. 277, p. 1956–1962.

Solomatov, V.S., and Barr, A.C., 2007, Onset of convection in fluids with strongly temperature-dependent, power-law viscosity, 2. dependence on the initial perturbation: Phys. Earth Planet. Inter., v. 165, p. 1–13.

Solomatov, V.S., and Moresi, L.N., 2000, Scaling of time-dependent stagnant lid convection: Application to small-scale convection on earth and other terrestrial planets: J. Geophys. Res., v. 105, p. 21,795–21,817.

Stein, C.A., and Stein, S., 1992, A model for the global variation in oceanic depth and heat flow with lithospheric age: Nature, v. 359, p. 123–129.

Tackley, P.J., 2000, Mantle convection and plate tectonics: Toward an integrated physical and chemical theory: Science, v. 288, p. 2002–2007.

Turcotte, D.L., and Oxburgh, E.R., 1967, Finite amplitude convective cells and continental drift: J. Fluid Mech., v. 28, p. 29–42.

Wen, L., and Anderson, D.L., 1997, Layered mantle convection: A model for geoid and topography: Earth Planet. Sci. Lett., v. 146, p. 367–377.

Yamamoto, J., Korenaga, J., Nirano, N., and Kagi, H., 2014, Melt-rich lithosphere-asthenosphere boundary inferred from petit-spot volcanoes: Geology, v. 42, p. 967–970.

Zhong, S., Ritzwoller, M., Shapiro, N., Landuyt, W., Huang, J., and Wessel, P., 2007, Bathymetry of the Pacific plate and its implications for thermal evolution of lithosphere and mantle dynamics: J. Geophys. Res., v. 112, p. B06,412, doi:10.1029/2006JB004,628.

Zlotnik, S., Afonso, J.C., Diez, P., and Fernandez, M., 2008, Small-scale gravitational instabilities under the oceans: Implications for the evolution of oceanic lithosphere and its expression in geophysical observables: Philos. Mag., v. 88, p. 1–11.

Jun Korenaga, Department of Geology and Geophysics, P.O. Box, 208109, Yale University, New Haven, CT 06520-8109. (jun.korenaga@yale.edu)

Received _____

This manuscript was prepared with AGU's LaTeX macros v5, with the extension package 'AGU++' by P. W. Daly, version 1.6b from 1999/08/19.

Figure Captions

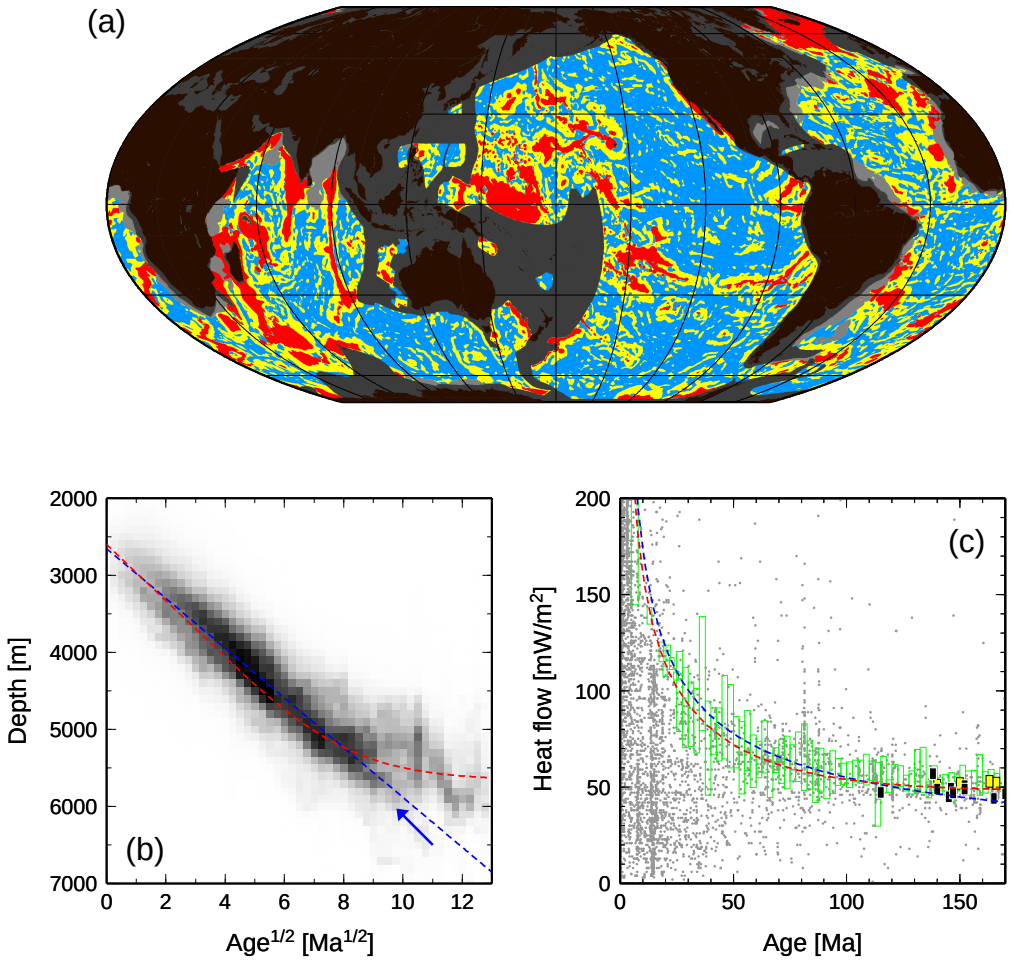

Figure 1. (a) Distribution of the normal seafloor according to the correlation criterion of Korenaga and Korenaga [2008] (shown in blue). Shown in red is the anomalous crustal region, characterized by residual depths of >1 km with respect to the plate model prediction of Stein and Stein [1992]. Yellow shading denotes regions with strong topographic correlation with the anomalous crust. Dark gray signifies whether either age or sediment data are unavailable, and light gray areas denote regions where sediment correction becomes inaccurate because of too thick (>2 km) sediments. (b) Age-depth relation for the normal seafloor according to the correlation criterion. Darker shading means larger area. Also shown are the predictions of the GDH1 plate model of Stein and Stein [1992] (red) and the best fit half-space cooling trend, $2654+323\sqrt{t}$, derived by Korenaga and Korenaga [2008] (blue). Blue arrow points to data that continue to follow the half-space cooling trend. (c) Age-heat flow relation. Grey dots shows all of available heat flow data [International Heat Flow Commission of IASPEI, 2011] for the normal seafloor. Red curve corresponds to the GDH1 plate model, and blue curve to half-space cooling with depth-dependent mantle properties ($q=550/\sqrt{t}$) [Korenaga and Korenaga, 2008]. Green boxes denote the compilation of Hasterok [2013], which is not restricted to the normal seafloor. Black and yellow boxes denote the compilation of Nagihara et al. [1996], and black boxes correspond to measurements on the normal seafloor.

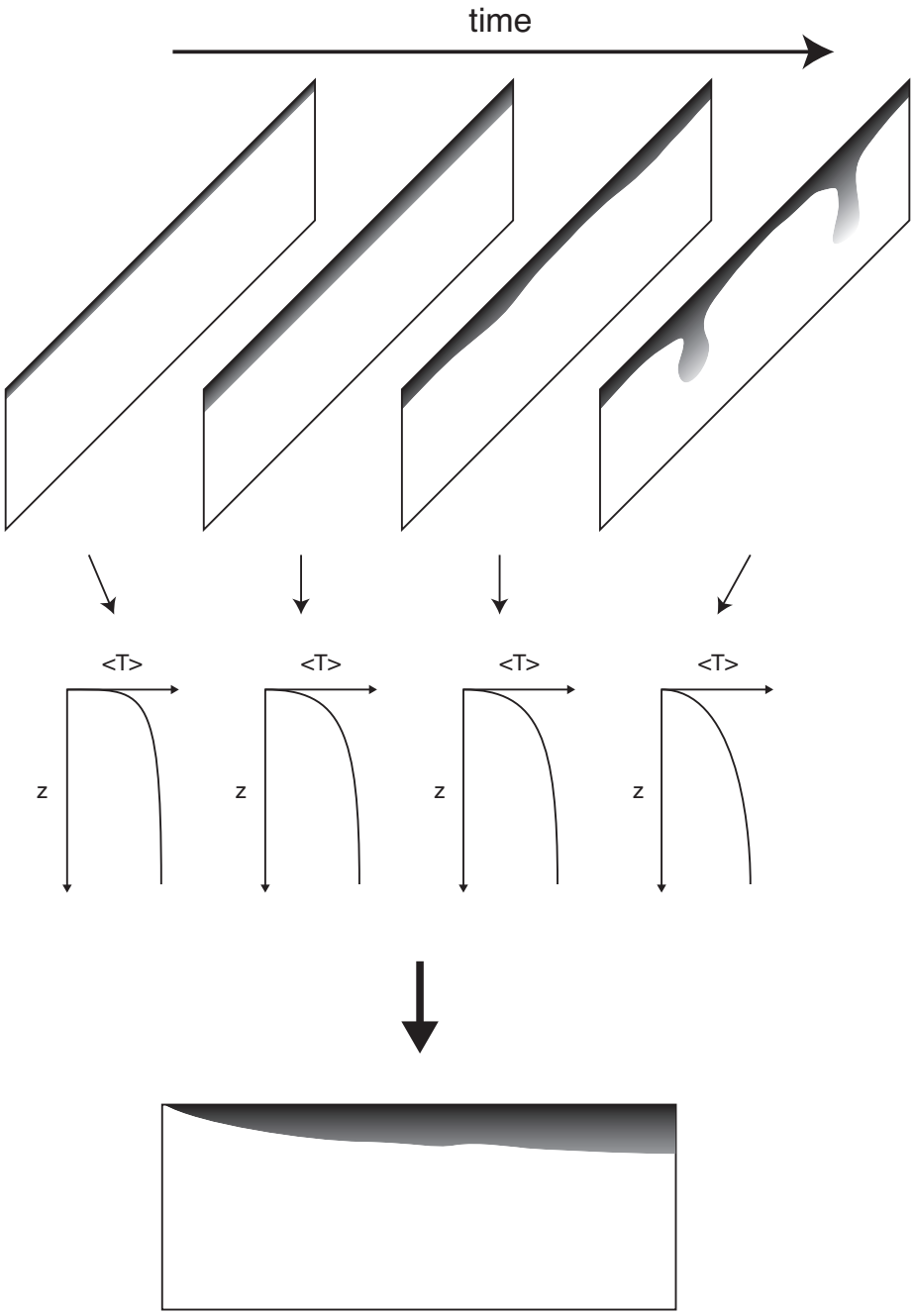

Figure 2. Schematic illustration for modelling strategy adopted in this study. A composite ridge-perpendicular thermal structure (bottom) is created by using horizontally-averaged temperature profiles calculated from a 2-D ridge-parallel convection model.

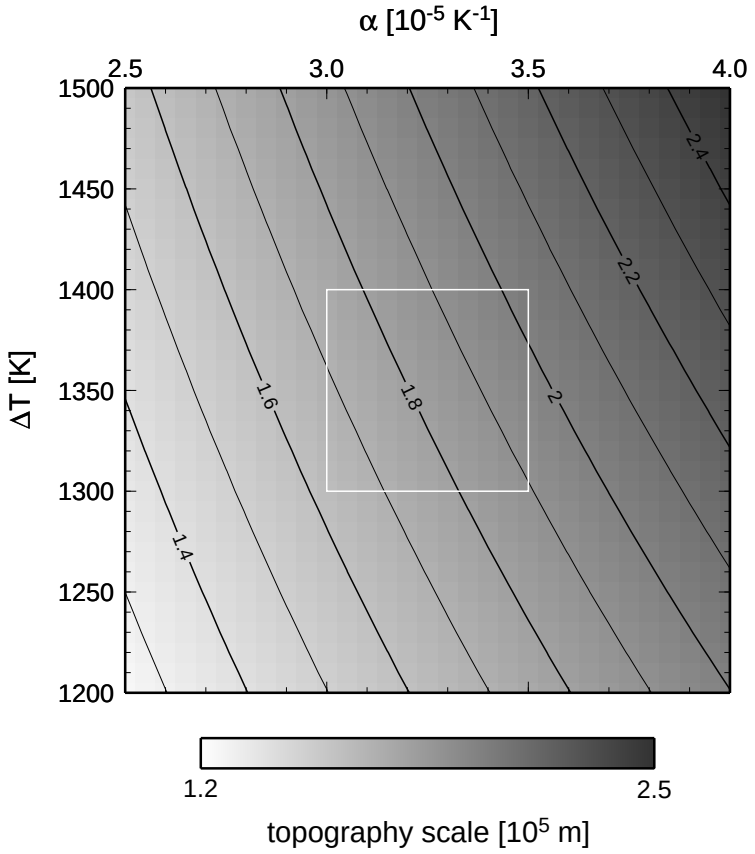

Figure 3. The topography scale as a function of the temperature scale and thermal expansivity [equation (10)]. A white box encloses the acceptable range for the present-day condition (see text).

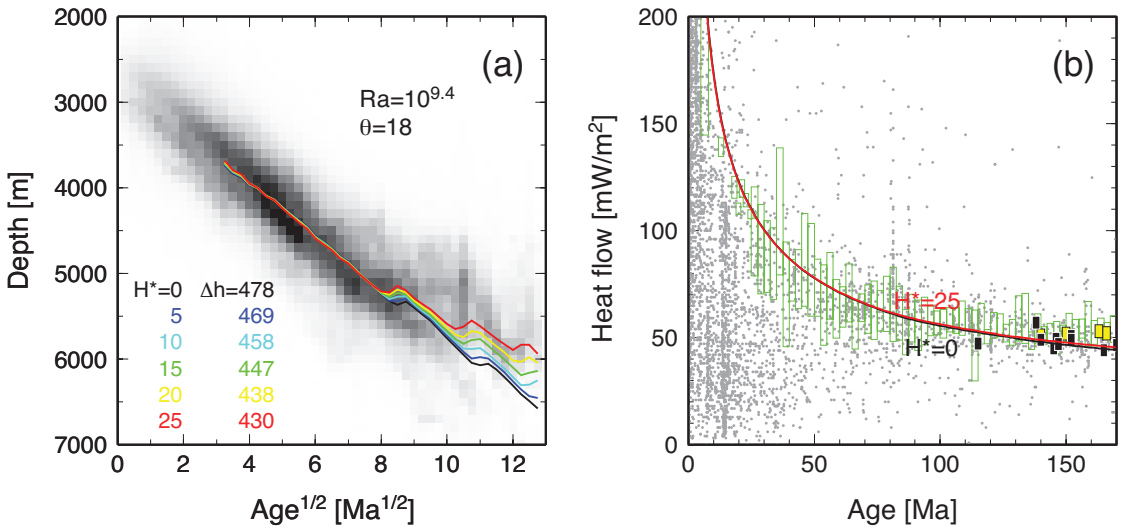

Figure 4. Comparison of dimensionalized model predictions with (a) the age-depth relation and (b) the age-heat flow relation. The cases of $Ra = 10^{9.4}$ and $\theta = 18$ are shown for a range of H^* (different colors correspond to different H^*). Data legend is the same as in Figure 1. The step-wise feature of model age-depth relations reflects instantaneous lithospheric delamination events in 1-D approximate solutions. Fully 2-D solutions do not exhibit this feature because of more gradual delamination (see Figure 7).

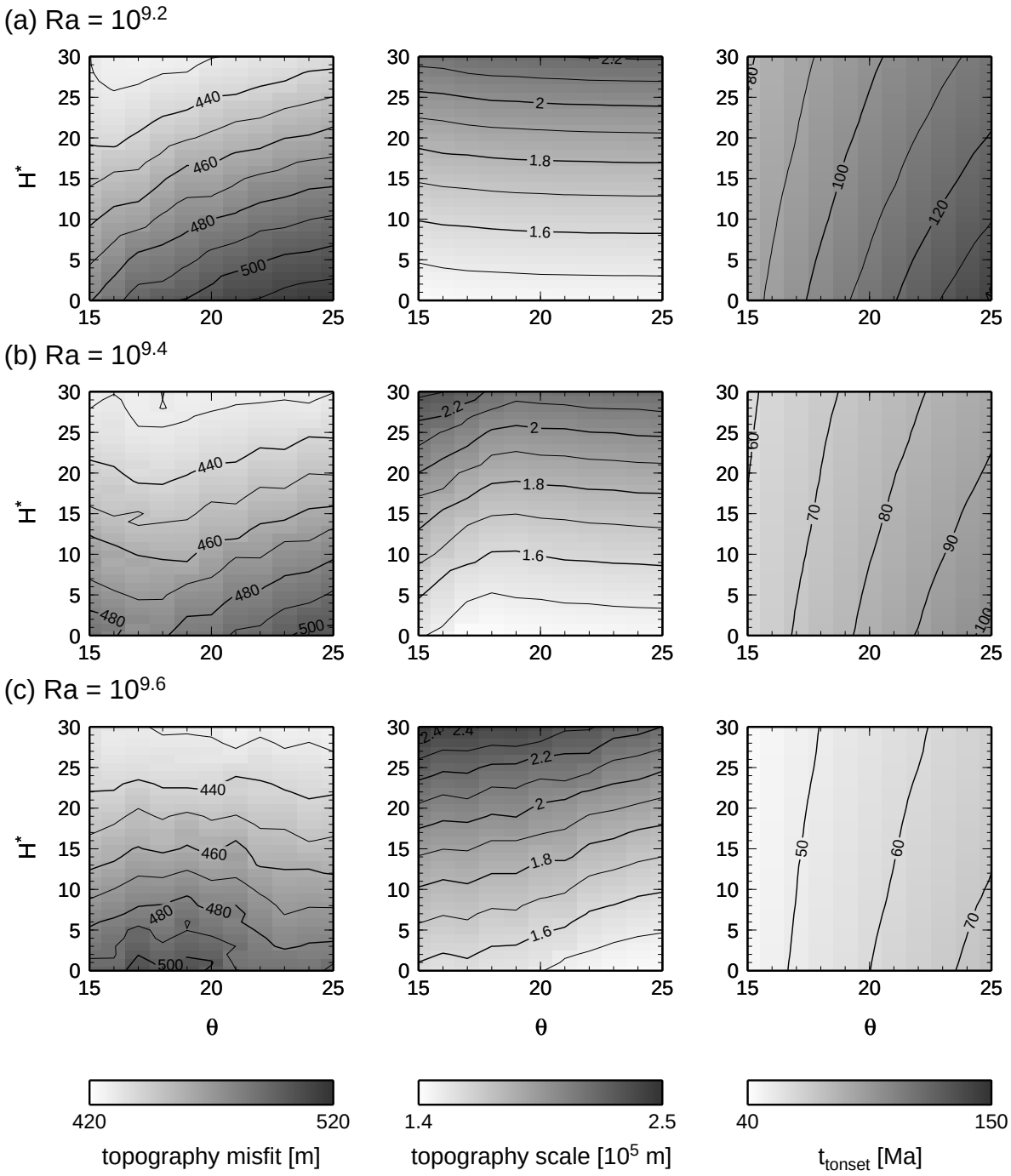

Figure 5. Results of grid search are shown for (a) $Ra = 10^{9.2}$, (b) $Ra = 10^{9.4}$, and (c) $Ra = 10^{9.6}$, in terms of the topography misfit (left column), the topography scale (middle), and the onset of convection (right).

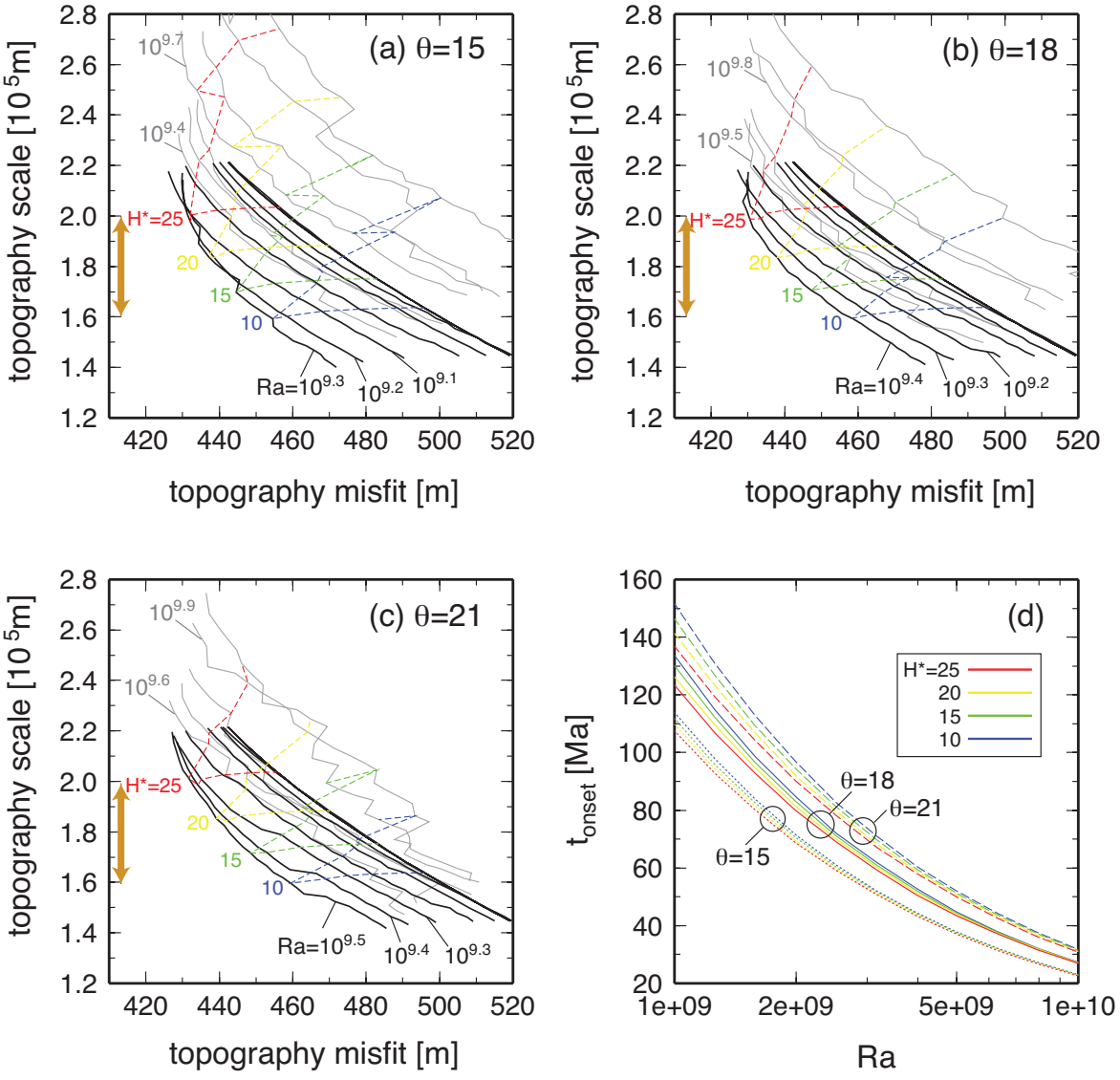

Figure 6. Trade-off between the topography misfit and the topography scale, summarized for (a) $\theta = 15$, (b) $\theta = 18$, and (c) $\theta = 21$. Solid and grey curves correspond to constant *Ra* values, whereas dashed curves to constant H^* values. Arrows signify the acceptable range of the topography scale. (d) Onset time of sublithospheric convection as a function of *Ra*.

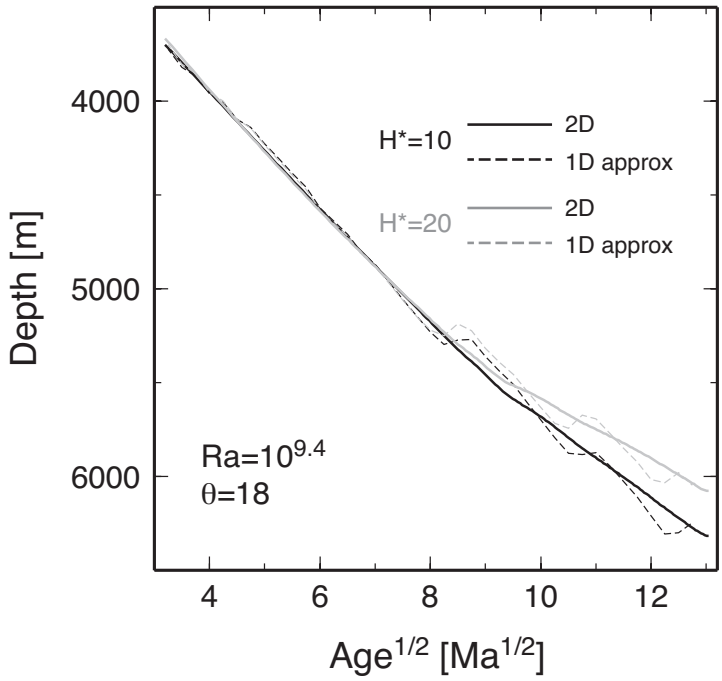

Figure 7. Comparison between 1-D approximate (dashed) and 2-D (solid) solutions in terms of surface topography, shown for the case of $Ra = 10^{9.4}$ and $\theta = 18$. For a given combination of model parameters, the same values of a_h and b_h are used for these two types of solutions.

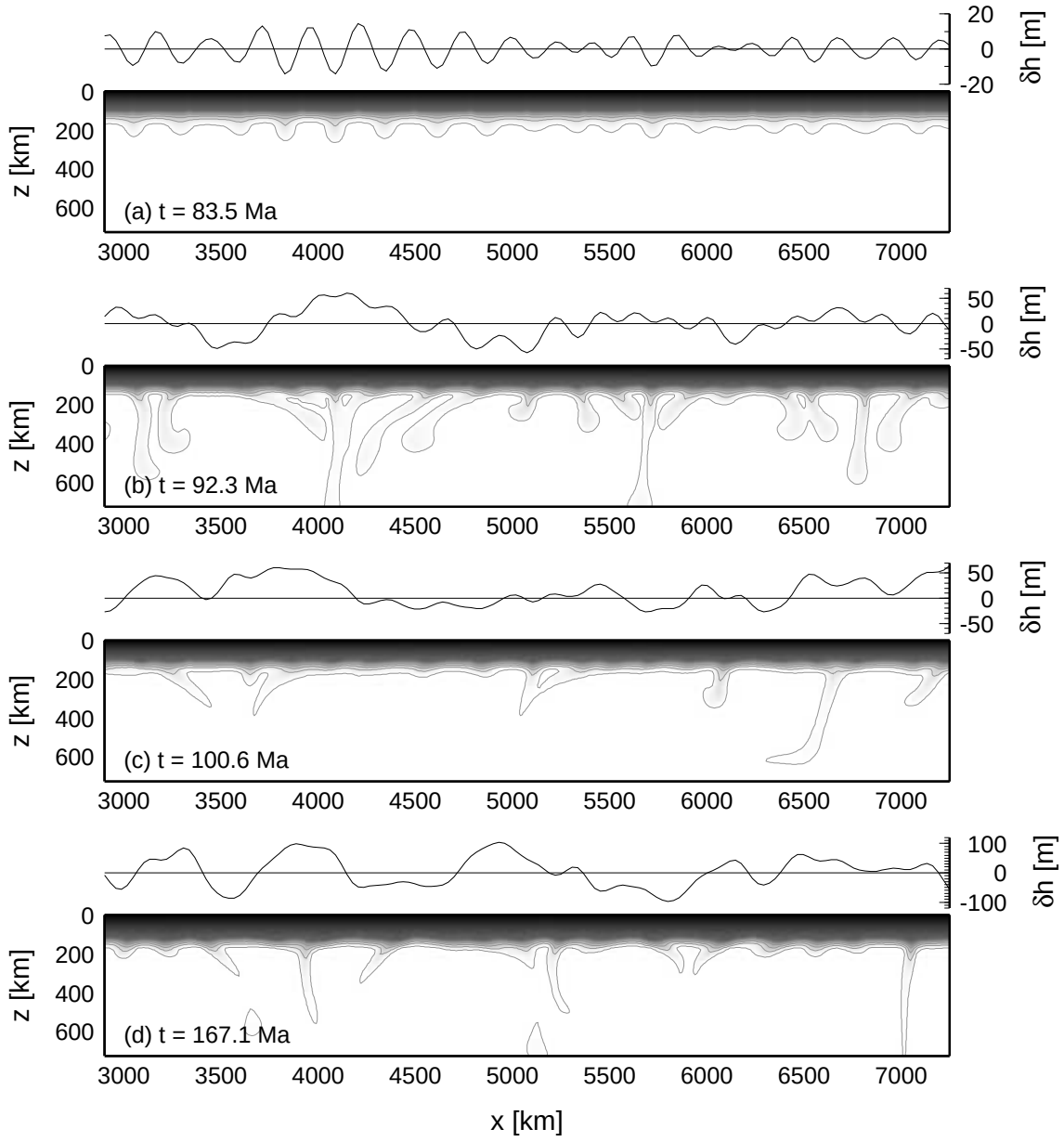

Figure 8. Snapshots of the temperature field from a 2-D ridge-parallel model for the case of $Ra = 10^{9.4}$, $\theta = 18$, and $H^* = 20$. Temperature is dimensionalized with $\Delta T = 1350$ K, and contours are drawn at every 50 K. To show the details of sublithospheric convection, only a small fraction of the total model domain ($4D \times D$, where $D = 2.9 \times 10^6$ m) is shown here. Corresponding surface topography is also shown.

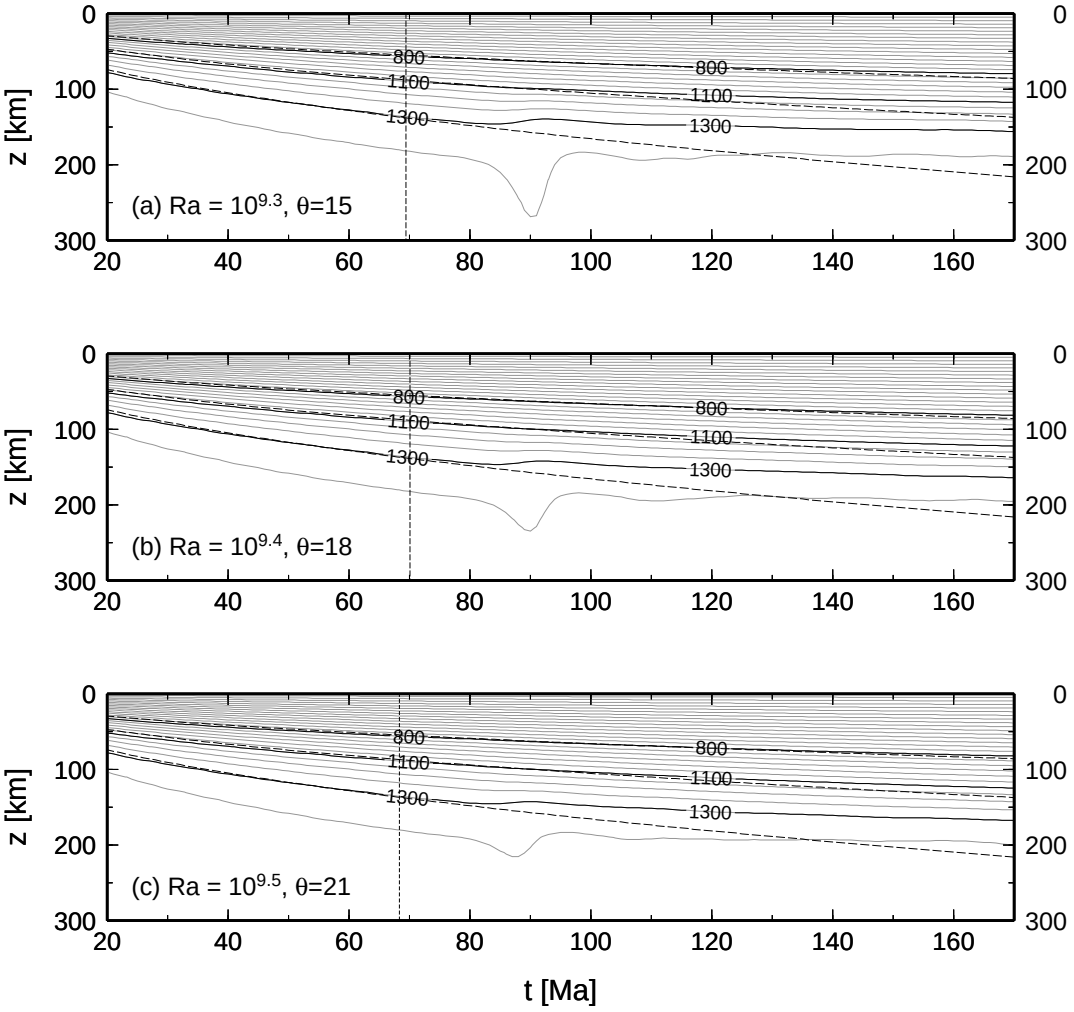

Figure 9. Ridge-perpendicular thermal structure based on 2-D ridge-parallel simulation, shown as a function of seafloor age for three representative optimal cases (a) $Ra = 10^{9.3}$ and $\theta = 15$, (b) $Ra = 10^{9.4}$ and $\theta = 18$, and (c) $Ra = 10^{9.6}$ and $\theta = 21$, all with $H^* = 20$. Only top 300 km is shown. Temperature is dimensionalized with $\Delta T = 1350$ K, and gray contours are drawn at every 50 K. Isotherms of 800 °C, 1100 °C, and 1300 °C are shown in solid. Also shown in dashed are isotherms according to simple half-space cooling (i.e., no internal heating). These temperatures are all potential temperature.

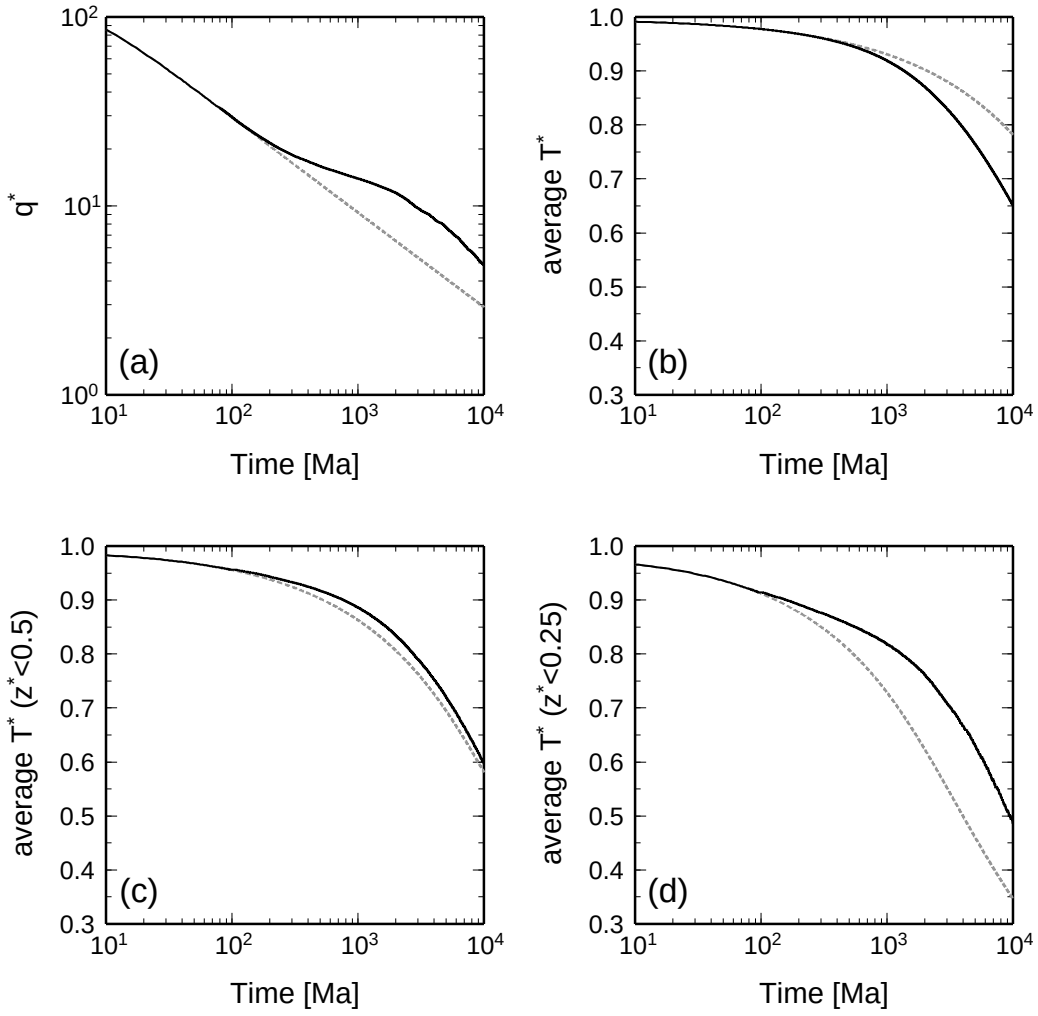

Figure 10. Additional modeling results to illustrate how small-scale convection enhances cooling with respect to a purely conducting case. A 2-D convection model similar to those described in the "A Close Look" section (θ=15 and $Ra = 10^{9.3}$) was run with no internal heating ($H^* = 0$), and results are shown in solid for (a) surface heat flux, (b) average temperature, (c) average temperature for the upper half of the model domain, and (c) average temperature for the upper quarter of the model domain. Also shown in dashed gray is the purely conducting case. Time axis is dimensionalized. The onset of convection takes place at $\sim$80 Ma, and its effect on surface heat flux becomes noticeable at $\sim$200 Ma, as predicted by Korenaga [2009a]. As seen in (b), the system as a whole cools faster than the conducting case, but the shallower portion of the system is warmer than the conducting case ((c) and (d)). This is because delaminated lithosphere sinks to the bottom of the mantle, and the lower portion of the system is cooled more efficiently. It can be seen that this trend continues at least to 10 Ga.